Evidence for Cu−O₂ Intermediates in Superoxide Oxidations by Biomimetic Copper(II) Complexes

Valeriy V. Smirnov and Justine P. Roth*

*Contribution from the Department of Chemistry, Johns Hopkins University,
3400 North Charles Street, Baltimore, Maryland 21218*

Received October 12, 2005; E-mail: jproth@jhu.edu

Abstract: The mechanism by which $[Cu^{II}(L)](OTf)_2$ and $[Cu^{II}N_3(L)](OTf)$ (L = TEPA: tris(2-pyridylethyl)-amine or TMPA: tris(2-pyridylmethyl)amine; OTf = trifluoromethanesulfonate) react with superoxide ($O_2^{\bullet-}$) to form $[Cu^I(L)](OTf)$ and O_2 is described. Evidence for a CuO_2 intermediate is presented based on stopped-flow experiments and competitive oxygen (^{18}O) kinetic isotope effects on the bimolecular reactions of $^{16,16}O_2^{\bullet-}$ and $^{18,16}O_2^{\bullet-}$ ($^{16,16}k/^{18,16}k$). The $^{16,16}k/^{18,16}k$ fall within a narrow range from 0.9836 ± 0.0043 to 0.9886 ± 0.0078 for reactions of copper(II) complexes with different coordination geometries and redox potentials that span a 0.67 V range. The results are inconsistent with a mechanism that involves either rate-determining $O_2^{\bullet-}$ binding or one-step electron transfer. Rather a mechanism involving formation of a CuO_2 intermediate prior to the loss of O_2 in the rate-determining step is proposed. Calculations of similar inverse isotope effects, using stretching frequencies of CuO_2 adducts generated from copper(I) complexes and O_2, suggest that the intermediate has a superoxo structure. The use of ^{18}O isotope effects to relate activated oxygen intermediates in enzymes to those derived from inorganic compounds is discussed.

Introduction

Metal ions are responsible for the acquisition of energy[1] and maintenance of homeostasis within the cell.[2−4] During aerobic respiration, chemical energy is harnessed from molecular oxygen by cytochrome *c* oxidase while other transition metal-mediated processes control the fluxes of the partially reduced O_2-derived products or *reactive oxygen species* (ROS).[5] Superoxide ion ($O_2^{\bullet-}$) is the primary ROS produced from O_2 and intracellular reductants according to eq 1.[6,7] Subsequent reactions afford hydroperoxyl radical ($HO_2^\bullet$), peroxynitrous acid ($HONO_2$) and hydrogen peroxide (H_2O_2).[5] These secondary ROS are believed to be involved in cell signaling pathways[8] as well as the oxidative damage of cellular sugars, lipids, proteins and DNA.[5,9]

$$O_2 + 1e^- \rightarrow O_2^{\bullet-} \qquad (1)$$

Transition metal ions in a variety of ligand environments have been implicated in the formation[10,11] as well as the scavenging of primary[6,7] and secondary ROS.[12−15] Yet only a handful of studies have provided compelling evidence for the mechanisms of these reactions.[12,16−19] In a variety of biological oxidations, including DNA cleavage[20,21] and enzymatic C−H oxidation,[22−24] the generation of reactive intermediates upon coordination of O_2 to mononuclear copper(I) sites has been proposed.[25] Whether the intermediates are electronically and structurally analogous to those formed when $O_2^{\bullet-}$ reacts with copper(II) centers has not been understood.

The majority of information concerning the structures of oxygen bound to a single copper center has come from studies of inorganic compounds.[31] Species with the formula $1Cu:1O_2$ have been synthesized by reacting O_2 with copper(I) complexes

(1) Babcock, G. T.; Wikstrom, M. *Nature* **1992**, *356*, 301.
(2) Luk, E.; Jensen, L. T.; Culotta, V. C. *J. Biol. Inorg. Chem.* **2003**, *8*, 803.
(3) O'Halloran, T. V.; Culotta, V. C. *J. Biol. Chem.* **2000**, *275*, 25057.
(4) Valentine, J. S.; Gralla, E. B. *Science* **1997**, *278*, 817.
(5) Halliwell, B. *Am. J. Med.* **1991**, *91 suppl 3C*, 14S.
(6) Miller, A.-F. In *Comprehensive Coordination Chemistry II: From Biology to Nanotechnology*; McCleverty, J. A., Meyer, T. J., Eds.; Elsevier Pergamon: Oxford, UK, 2004; Vol. 8, p 479.
(7) Cabelli, D. E.; Riley, D.; Rodriguez, J. A.; Valentine, J. S.; Zhu, H. in *Biomimetic Oxidations Catalyzed by Transition Metal Complexes*; Meunier, B., Ed.; Imperial College Press: London, UK, 2000; p 461.
(8) Montagnier, L., Olivier, R., Pasquier, C., Eds. *Oxidative Stress in Cancer, Aids, and Neurodegenerative Diseases*; Marcel Dekker: New York, 1998.
(9) Martindale, J. L.; Holbrook, N. J. *J. Cell. Physiol.* **2002**, *192*, 1.
(10) Whittaker, J. W. *Chem. Rev.* **2003**, *103*, 2347.
(11) Klinman, J. P. *J. Biol. Inorg. Chem.* **2001**, *6*, 1.
(12) Dunford, H. B. *Heme Peroxidases*; Wiley-VCH: New York, 1999.

(13) Wu, A. J.; Penner-Hahn, J. E.; Pecoraro, V. L. *Chem. Rev.* **2004**, *104*, 903.
(14) Goldstein, S.; Lind, J.; Merenyi, G. *Chem. Rev.* **2005**, *105*, 2457.
(15) Herold, S.; Koppenol, W. H. *Coord. Chem. Rev.* **2005**, *249*, 499.
(16) Weinstein, J.; Bielski, B. H. J. *J. Am. Chem. Soc.* **1980**, *102*, 4916.
(17) Cabelli, D. E.; Bielski, B. H. J.; Holcman, J. *J. Am. Chem. Soc.* **1987**, *109*, 3665.
(18) Fee, J. A.; Bull, C. *J. Biol. Chem.* **1986**, *261*, 13000.
(19) Boccini, F.; Herold, S. *Biochemistry* **2004**, *43*, 16393.
(20) Cowan, J. A. *Curr. Opin. Chem. Biol.* **2001**, *5*, 634.
(21) Chen, C.-h. B.; Milne, L.; Landgraf, R.; Perrin, D. M.; Sigman, D. S. *ChemBioChem* **2001**, *2*, 735.
(22) Chen, P.; Solomon, E. I. *J. Am. Chem. Soc.* **2004**, *126*, 4991.
(23) Evans, J. P.; Ahn, K.; Klinman, J. P. *J. Biol. Chem.* **2003**, *278*, 49691.
(24) Klinman, J. P. *Chem. Rev.* **1996**, *96*, 2541.
(25) The formation of oxidizing species upon reductive activation of O_2 at dicopper sites has been discussed for tyrosinase (ref 26) and particulate methane monooxygenase (ref 27). The reaction is well established in model systems (refs 28−30).
(26) Solomon, E. I.; Baldwin, M. J.; Lowery, M. D. *Chem. Rev.* **1992**, *92*, 521.
(27) Lieberman, R. L.; Rosenzweig, A. C. *Nature* **2005**, *434*, 177.
(28) Lewis, E. A.; Tolman, W. B. *Chem. Rev.* **2004**, *104*, 1047.
(29) Itoh, S.; Fukuzumi, S. *Bull. Chem. Soc. Jpn.* **2002**, *75*, 2081.
(30) Mirica, L. M.; Vance, M.; Rudd, D. J.; Hedman, B.; Hodgson, K. O.; Solomon, E. I.; Stack, T. D. P. *Science* **2005**, *308*, 1890.
(31) Cramer, C. J.; Tolman, W. B.; Theopold, K. H.; Rheingold, A. L. *Proc. Natl. Acad. Sci. U.S.A.* **2003**, *100*, 3635.
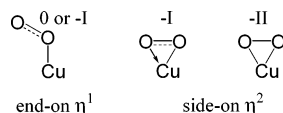
Figure 1. 1:1 copper−oxygen adducts. Roman numerals represent formal oxidation states corresponding to dioxygen (0), superoxide (−I) and peroxide (−II).

at low temperatures (ca. −80 °C).[32−37] Spectroscopic and/or X-ray crystallographic studies have provided evidence for end-on (η^1) superoxo[38,39] structures as well as the side-on (η^2) superoxo[36] and peroxo[37,40] structures (Figure 1). Although transient CuO_2 intermediates have been proposed to form upon reacting $O_2^{\bullet-}$ and copper(II),[16,17,41−45] none of these has been structurally characterized. In fact, no crystal structures of η^1-CuO_2 complexes derived from inorganic compounds have been reported to date.[46] These species are generally viewed as unstable with respect to the loss of O_2. The η^2-CuO_2 species are considered to be more stable like the well-known peroxo compounds derived from group IX and X transition metals.[37,47] Computational investigations have suggested these complexes have electronic ground states with differing contributions from resonance forms formally described as $Cu^I-O_2^{0}$, $Cu^{II}-O_2^{-I}$, and $Cu^{III}-O_2^{-II}$.[31,48] Because of their oversimplified nature, the use of oxidation state formalisms in reference to CuO_2 species is deemphasized throughout most of this article.

The relationship of electronic to vibrational structure in inorganic oxygen complexes has been and continues to be a thoroughly investigated area.[31,49] As a complement to such studies, we are developing new mechanistic probes which can correlate structure to reactivity in enzymes and biomimetic systems. This type of correlation is central to understanding the catalytic mechanisms of several copper-containing enzymes including peptidylglycine α-hydroxylating monooxygenase (PHM),[22−24,38] dopamine β-monooxygenase (DβM),[22,50] tyrosinase,[26] particulate methane monooxygenase[27] and Cu:Zn superoxide dismutase (Cu:Zn SOD).[51]

Determining the identities of the reactive intermediates in the enzymes is a particularly challenging problem. Much progress has recently been made for PHM which like DβM is a member of a family of structurally homologous copper proteins responsible for the biosynthesis of hormones and neurotransmitters.[24] Reduced copper(I) forms of PHM and DβM are believed to bind O_2 and generate reactive CuO_2 intermediates which stereoselectively oxidize substrate C−H bonds by hydrogen atom abstraction.[52] Related CuO_2 species have also been proposed to form transiently in Cu:Zn SOD upon reaction of $O_2^{\bullet-}$ with the oxidized copper(II) enzyme. Release of O_2 from this intermediate is proposed to occur spontaneously, prior to the reaction of copper(I) with a second equivalent of $O_2^{\bullet-}$. An alternative mechanism has also been considered wherein a CuO_2 intermediate reacts with a second equivalent of $O_2^{\bullet-}$ to afford O_2 and a copper(II) peroxo product which is subsequently hydrolyzed to H_2O_2.[51,53] These examples illustrate how differing reactivity patterns have been attributed to CuO_2 intermediates; the activated oxygen ligand is unstable with respect to oxidation in SOD and with respect to reduction by exogenous substrates in PHM and DβM.

This study explores the mechanism by which $O_2^{\bullet-}$ is oxidized to O_2 by biomimetic copper(II) complexes. Competitive oxygen (^{18}O) isotope fractionation techniques are used to provide evidence for intermediates during these reactions. The measurements employ stable isotope mass spectrometry to determine changes in the ratio of heavy to light isotopes from their natural abundance levels.[54] The technique has been used extensively in the atmospheric and geological sciences. With respect to biological reactions, early work by Berry[55,56] and by Epstein[57] demonstrated fractionation during respiration, although the results were not interpreted in terms of the underlying redox chemistry.

The use of competitive ^{18}O kinetic isotope effects (KIEs) to probe reactions of O_2 is described in two recent reviews.[58,59] In addition, we have recently reported studies of ^{18}O KIEs on O_2 activation by classic inorganic compounds.[47] Described here is, to our knowledge, the first extension of the competitive isotope fractionation technique to reactions of $O_2^{\bullet-}$. These studies lay a foundation for applying ^{18}O KIEs to probe mechanisms by which reactive oxygen species are processed by metalloenzymes. A key aspect of the approach is the use of isotope effects to compare structurally and spectroscopically defined biomimetic compounds to metal-activated oxygen intermediates in enzymes.

Experimental Methods

All manipulations of moisture- and oxygen-sensitive compounds were carried out using standard high-vacuum techniques or a N_2-filled glovebox (MBraun). Potassium superoxide (KO_2) was obtained as a

(32) Fry, H. C.; Scaltrito, D. V.; Karlin, K. D.; Meyer, G. J. *J. Am. Chem. Soc.* **2003**, *125*, 11866.
(33) Zhang, C. X.; Kaderli, S.; Costas, M.; Kim, E.-i.; Neuhold, Y.-M.; Karlin, K. D.; Zuberbuehler, A. D. *Inorg. Chem.* **2003**, *42*, 1807.
(34) Wei, N.; Murthy, N. N.; Chen, Q.; Zubieta, J.; Karlin, K. D. *Inorg. Chem.* **1994**, *33*, 1953.
(35) Karlin, K. D.; Wei, N.; Jung, B.; Kaderli, S.; Niklaus, P.; Zuberbuehler, A. D. *J. Am. Chem. Soc.* **1993**, *115*, 9506.
(36) Fujisawa, K.; Tanaka, M.; Moro-oka, Y.; Kitajima, N. *J. Am. Chem. Soc.* **1994**, *116*, 12079.
(37) Tolman, W. B. et al. *J. Am. Chem. Soc.* **2004**, *126*, 16896.
(38) Prigge, S. T.; Eipper, B. A.; Mains, R. E.; Amzel, L. M. *Science* **2004**, *304*, 864.
(39) Schatz, M.; Raab, V.; Foxon, S. P.; Brehm, G.; Schneider, S.; Reiher, M.; Holthausen, M. C.; Sundermeyer, J.; Schindler, S. *Angew. Chem., Int. Ed. Eng.* **2004**, *43*, 4360.
(40) Reynolds, A. M.; Gherman, B. F.; Cramer, C. J.; Tolman, W. B. *Inorg. Chem.* **2005**, *44*, 6989.
(41) Luo, Q.-H.; Zhang, J.-J.; Hu, X.-L.; Jiang, X.-Q.; Shen, M.-C.; Li, F.-M. *Inorg. Chim. Acta* **2004**, *357*, 66.
(42) Nishida, Y.; Unoura, K.; Watanabe, I.; Yokomizo, T.; Kato, Y. *Inorg. Chim. Acta* **1991**, *181*, 141.
(43) Bailey, C. L.; Bereman, R. D.; Rillema, D. P. *Inorg. Chem.* **1986**, *25*, 3149.
(44) Nappa, M.; Valentine, J. S.; Miksztal, A.; Schugar, H. J.; Isied, S. S. *J. Am. Chem. Soc.* **1979**, *101*, 7744.
(45) Meisel, D.; Levanon, H.; Czapski, G. *J. Phys. Chem.* **1974**, *78*, 779.
(46) Aboelella, N. W.; Reynolds, A. M.; Tolman, W. B. *Science* **2004**, *304*, 836.
(47) Lanci, M.; Brinkley, D. W.; Stone, K. L.; Smirnov, V. V.; Roth, J. P. *Angew. Chem., Int. Ed. Eng.* **2005**, *44*, 7273.
(48) Gherman, B. F.; Cramer, C. J. *Inorg. Chem.* **2004**, *43*, 7281.
(49) Lever, A. B. P.; Ozin, G. A.; Gray, H. B. *Inorg. Chem.* **1980**, *19*, 1823.
(50) Tian, G.; Berry, J. A.; Klinman, J. P. *Biochemistry* **1994**, *33*, 226 and 14650.
(51) Hart, P. J.; Balbirnie, M. M.; Ogihara, N. L.; Nersissian, A. M.; Weiss, M. S.; Valentine, J. S.; Eisenberg, D. *Biochemistry* **1999**, *38*, 2167.

(52) Francisco, W. A.; Blackburn, N. J.; Klinman, J. P. *Biochemistry* **2003**, *42*, 1813.
(53) Osman, R.; Basch, H. *J. Am. Chem. Soc.* **1984**, *106*, 5710.
(54) McKinney, C. R.; McCrea, J. M.; Epstein, S.; Allen, H. A.; Urey, H. C. *Rev. Sci. Instrum.* **1950**, *21*, 724.
(55) Guy, R. D.; Fogel, M. F.; Berry, J. A.; Hoering, T. C. In *Progress in Photosynthesis Research, Proceedings of the 7th International Congress on Photosynthesis*; Biggins, J., Ed.; Martinus Nijhoff Publishers: Dordrect, The Netherlands, 1987; Vol. 3, p 597.
(56) Guy, R. D.; Berry, J. A.; Fogel, M. L.; Hoering, T. C. *Planta* **1989**, *177*, 483.
(57) Epstein, S.; Zeiri, L. *Proc. Natl. Acad. Sci. U.S.A.* **1988**, *85*, 1727.
(58) Roth, J. P.; Klinman, J. P. in *Isotope Effects in Chemistry and Biology*; Kohen, A., Limbach, H. H., Eds.; CRC Press: Boca Raton, FL, 2005; p 645.
(59) Smirnov, V. V.; Brinkley, D. W.; Lanci, M. P.; Karlin, K. D.; Roth, J. P. *J. Mol. Catal. A* **2006**, accepted.

yellow powder from Aldrich (45.04% O by weight) and used as received. 18-crown-6 ether was obtained from Aldrich (99.9% purity) and dried over P_2O_5 in vacuo for several days prior to use. Ferricytochrome *c* from bovine heart and manganese superoxide dismutase from *E. coli* were obtained from Sigma and used as received. Tetra-*n*-butylamonium hexafluorophosphate (^{n}Bu₄NPF₆) was obtained from Strem Chemicals and dried in vacuo over P_2O_5 prior to use. Ferrocene (TCI America) was sublimed prior to use in electrochemical experiments. "Anhydrous" grade DMSO and DMF solvents were obtained from Burdick and Jackson and used without further purification. DMF was stored in the dark at −30 °C. Tetrahydrofuran (THF) was stored over sodium/benzophenone and vacuum distilled prior to use. Acetonitrile (CH_3CN) was dried and purified by two vacuum distillations, first from calcium hydride and then from P_2O_5. Deionized water was purified to 18 MΩ by passing through a Millipore Milli-Q system.

Copper complexes were synthesized according to modified literature procedures.[60,61] Samples were dried in vacuo over P_2O_5 for 24 h prior to use. Purity was checked by comparison with reported extinction coefficients and elemental analysis (Desert Analytics, Tucson, AZ). Cu(TEPA)OTf₂ {**Cu^{II}(TEPA)**} (TEPA = tris(2-pyridylethyl)amine and OTf = trifluoromethanesulfonate): Anal. Calcd for $C_{23}H_{24}N_4O_6F_6S_2Cu$: C, 39.80; H, 3.49; N, 8.07. Found: C, 39.83; H, 3.34; N, 7.96. Cu(TEPA)OTf {**Cu^{I}(TEPA)**}: Anal. Calcd for $C_{22}H_{24}N_4O_3F_3SCu$: C, 48.48; H, 4.44; N, 10.28. Found: C, 48.39; H, 4.65; N, 10.15. CuN₃-(TEPA)OTf {**Cu^{II}N₃(TEPA)**}: Anal. Calcd for $C_{22}H_{24}N_7O_3F_3SCu$: C, 45.01; H, 4.12; N, 16.70. Found: C, 45.07; H, 3.97; N, 16.38. Cu(TMPA)OTf₂ {**Cu^{II}(TMPA)**} (TMPA: tris(2-pyridylmethyl)amine): Anal. Calcd for $C_{20}H_{18}N_4O_6F_6S_2Cu$: C, 36.84; H, 2.78; N, 8.59. Found: C, 36.30; H, 2.87; N, 8.46. CuN₃(TMPA)OTf {**Cu^{II}N₃(TMPA)**}: Anal. Calcd for $C_{19}H_{18}N_7O_3F_3SCu$: C, 41.87; H, 3.33; N, 17.99. Found: C, 41.78; H, 3.21; N, 17.85. An analytically pure sample of [Cu^I(TMPA)](PF₆) {**Cu^I(TMPA)**}[62] was provided by Prof. Kenneth D. Karlin. The following molar absorptivities were determined in DMSO: **Cu^{II}(TEPA)** ϵ = 15 100 ± 300 M⁻¹ cm⁻¹ (λ_{max} = 263 nm), **Cu^I(TEPA)** ϵ = 9300 ± 120 M⁻¹ cm⁻¹ (λ_{max} = 345 nm), **Cu^{II}N₃(TEPA)** ϵ = 2500 ± 110 M⁻¹ cm⁻¹ (λ_{max} = 411 nm), **Cu^{II}N₃(TMPA)** ϵ = 3400 ± 130 M⁻¹ cm⁻¹ (λ_{max} = 412 nm).

NMR spectra were recorded using Bruker Avance 400 MHz FT-NMR spectrometers. Chemical shifts (δ) are reported relative to residual protio signals of the deuterated solvent. UV−vis spectra were recorded on an Agilent 8453 UV−vis spectrophotometer. The cell temperature was controlled with a Peltier 89090-A. Room-temperature stopped-flow kinetic measurements were performed on an OLIS RSM 1000 spectrophotometer equipped with a 1 cm observation cell. The spectrophotometer was installed in a N₂-filled double-length glovebox (MBraun). Low-temperature stopped-flow experiments were conducted on SF-40 Hi-Tech Scientific stopped-flow system equipped with a 1 cm path length cell, NMC 301 diode array detector (J & M, 300−1100 nm range, 1.3 ms sampling time) and flexible light guides connected to a CLX 75 W xenon lamp. Cyclic voltammetry was carried out using a Bioanalytical Systems BAS 100B electrochemical analyzer. The concentration of O₂ in aqueous samples was determined using a Clark electrode (Biological Oxygen Monitor 5300A, YSI). The ^{18}O/^{16}O ratio in CO_2 samples was determined using a Micromass stable isotope mass spectrometer equipped with a dual inlet system. Isotope ratio mass spectrometry services were provided by facilities at Johns Hopkins University and the University of Maryland, College Park.

Preparation of Superoxide Solutions. All glassware was rinsed with Milli-Q (18MΩ) water and rigorously dried. Solutions of KO₂ in anhydrous DMSO or DMF were freshly prepared under N₂ just before use. Care was taken to protect solutions from moisture and to remove

residual O₂. A typical procedure involved suspending solid KO₂ (26 mg) in DMSO (100 mL) and, after 25 min of stirring, filtering the solution through a Corning nylon membrane with 0.2 μm pore size. A clear, pale yellow solution was obtained. 18-Crown-6 ether (67 mg) was used to solubilize KO₂ (18 mg) in cold DMF (20 mL). The suspension was stirred for 3 min and filtered through a nylon membrane. The solution was diluted with DMF or DMF/THF (28 mL DMF/12 mL THF) for use in the low-temperature stopped-flow experiments.

The concentration of O₂$^{\bullet -}$ was determined by injecting a 10 μL aliquot of N₂-saturated solution into 1.00 mL aqueous solution of ferricytochrome *c* or ferricytochrome *c* + Mn SOD (pH 10 NaHCO₃ buffer, 10⁻⁴ M EDTA). The concentration of O₂$^{\bullet -}$ was calculated from the SOD-inhibitable activity indicated by Clark electrode readings.[63] A calibration curve was prepared by correlating the concentrations of O₂$^{\bullet -}$ to UV absorbance measurements using a 0.1 cm path length quartz cell. Beer's law analysis indicated an extinction coefficient $\epsilon_{254\ nm}$ = 4200 ± 200 M⁻¹cm⁻¹ for O₂$^{\bullet -}$ in DMSO, which is somewhat higher than previously reported values.[64−66] Protected from moisture, these solutions were stable for more than 12 h at room temperature. Only a 4% drop in the concentration of O₂$^{\bullet -}$ was detected by spectrophotometry and by manometry on the O₂ produced from a standard reaction (see below). Solutions of O₂$^{\bullet -}$ in DMF were less stable and decayed by 20% over the course of 6 h. For this reason, KIE measurements were performed with DMSO as the solvent.

Synthesis of Co^{III}(SMDPT)OTf·H₂O for Use as a Calibration Standard. Co^{III}(SMDPT)OTf·H₂O {**Co^{III}(SMDPT)**} (SMDPT = bis-(salicylidene-γ-iminopropyl)methylamine) was prepared by oxidation of Co^{II}(SMDPT)[67] with an equimolar amount of AgOTf in CH_3CN. The AgOTf in anhydrous CH_3CN was added slowly to a stirred solution of Co^{II}(SMDPT) in CH_3CN protected from light. The reaction mixture was allowed to stir overnight. The Ag^0 produced was removed by several filtrations through diatomaceous earth (Celite 521) and a 0.2 μm nylon membrane. The CH_3CN was removed by rotary evaporation. The remaining black residue was purified by multiple crystallizations from CH_2Cl_2/Et₂O. The final product had an appearance of dark red needles without any metallic shine. The yield of **Co^{III}(SMDPT)** after recrystallization and drying in vacuo was 64%. ^{1}H NMR (400 MHz, CD₃CN) δ 7.99 (1H, s), 7.85 (1H, s), 7.29 (2H, t, *J* = 8 Hz), 7.15 (2H, br t), 7.00 (1H, br s), 6.93 (1H, d, *J* = 8 Hz), 6.63 (1H, t, *J* = 8 Hz), 6.58 (1H, t, *J* = 8 Hz), 5.46 (2H, very br s, H₂O−Co), 3.60 (1H, br t, *J* = 12 Hz), 3.44 (1H, t, *J* = 12 Hz), 3.14 (1H, dt, J_1 = 4 Hz, J_2 = 13 Hz), 2.61 (1H, br t), 2.30 (1H, m), 2.10 (5H, m), 1.70 (3H, s, H_3C), 1.60 (2H, m); UV−vis (DMSO): λ_{max} = 385 nm, ϵ = 4700 ± 400 M⁻¹cm⁻¹. Anal. Calcd. for $C_{22}H_{27}N_3O_6F_3SCo$: C, 45.76; H, 4.71; N, 7.28. Found: C, 45.93; H, 4.71; N, 7.25.

The reaction of 1−3 equiv. of **Co^{III}(SMDPT)** with 1 equivalent of O₂$^{\bullet -}$ in DMSO resulted in a 101 ± 4% yield of O₂ by manometry and a 93 ± 11% yield of Co^{II}(SMPDT) based on its optical absorbance spectrum (λ_{max} = 350 nm, ϵ = 12500 ± 2000 M⁻¹cm⁻¹).[68] This reaction, which proceeds quantitatively, was used to determine both the concentration of O₂$^{\bullet -}$ in solution as well as the initial isotope composition of this nonenriched reactant (see below).

Determination of Isotope Effects. The apparatus and basic methodology used to determine competitive oxygen kinetic isotope effects has been previously described.[58,59] Since the present studies include, to our knowledge, the first measurements to be performed on reactions of O₂$^{\bullet -}$ a brief overview is provided. A collapsible Tedlar bag (MiDan company, Chino, CA) was used as the reaction vessel to accommodate the use of organic solvents. Under N₂, an assembly consisting of a

(60) Karlin, K. D.; Hayes, J. C.; Hutchinson, J. P.; Hyde, J. R.; Zubieta, J. *Inorg. Chim. Acta* **1982**, *64*, L219.
(61) Karlin, K. D.; Hayes, J. C.; Juen, S.; Hutchinson, J. P.; Zubieta, J. *Inorg. Chem.* **1982**, *21*, 4106.
(62) Tyeklar, Z.; Jacobson, R. R.; Wei, N.; Murthy, N. N.; Zubieta, J.; Karlin, K. D. *J. Am. Chem. Soc.* **1993**, *115*, 2677.
(63) Fridovich, I. *J. Biol. Chem.* **1970**, *245*, 4053.
(64) Kim, S.; DiCosimo, R.; San Filippo, J., Jr. *Anal. Chem.* **1979**, *51*, 679.
(65) Gampp, H.; Lippard, S. J. *Inorg. Chem.* **1983**, *22*, 357.
(66) Sawyer, D. T.; Calderwood, T. S.; Yamaguchi, K.; Angelis, C. T. *Inorg. Chem.* **1983**, *22*, 2577.
(67) Bailes, R. H.; Calvin, M. *J. Am. Chem. Soc.* **1947**, *69*, 1886.
(68) Drago, R. S.; Cannady, J. P.; Leslie, K. A. *J. Am. Chem. Soc.* **1980**, *102*, 6014.

resealable round-bottom flask, two-way crossover stopcock and solvent impervious bag was charged with the $O_2^{\bullet-}$ solution. After connecting to the vacuum line, both the bag and the solution in the round-bottom flask were purged with He gas for 30 min to remove any residual O_2. The bag was filled with the $O_2^{\bullet-}$ solution while displacing the He gas. $Co^{III}(SMDPT)$ in DMSO (20 mg in 1.5 mL) was placed in a gas bubbler, attached to the vacuum manifold and then degassed. The vacuum apparatus was prepared for sample collection by evacuation to $\sim$10 milliTorr.

In a typical measurement, a calibrated tube built into the vacuum apparatus was filled with the $O_2^{\bullet-}$ solution. This solution was dispensed to the bubbler containing the $Co^{III}(SMDPT)$ standard. Immediately, the mixture was vigorously purged with He gas under dynamic vacuum for 20 min to remove O_2 and collect it in a molecular sieve trap cooled to -196 °C with liquid N_2. Excess He was released under reduced pressure prior to liberating O_2 from the sieves by warming with hot water. The O_2 was then recirculated through a combustion furnace and the CO_2, which formed quantitatively, condensed into a liquid nitrogen-cooled finger. The CO_2 was then recondensed into a fixed-volume part of the vacuum apparatus. Its pressure was accurately measured with a capacitance manometer (Omega PX238 with U24Y101 Linear Power Supply) calibrated using predetermined amounts of O_2. The CO_2 sample was sealed under vacuum in a dry glass tube for isotope ratio mass spectrometry analysis. These measurements provided the $^{18}O/^{16}O$ composition of the nonenriched $O_2^{\bullet-}$.

Reactions between $O_2^{\bullet-}$ and copper complexes were performed as described above for the standard reaction of $Co^{III}(SMDPT)$ except that substoichiometric quantities of the oxidant were used. In a typical set of measurements, two standard reactions and four measurements with the copper complexes were performed. The concentrations of the $O_2^{\bullet-}$ solution determined from the standard reaction at the beginning and end of the day were typically within 4%. Changes in $O_2^{\bullet-}$ concentration due to reactions with copper complexes were determined according to: $f = P_{CO_2(Cu)}/P_{CO_2(standard)}$, where P is the pressure of CO_2, and f is the fraction of O_2 produced.

Electrochemistry. Cyclic voltammetry was performed using a three-electrode setup consisting of a working glassy carbon electrode, a platinum wire counter electrode, and Ag/Ag$^+$ reference electrode (0.01 M AgNO$_3$ in DMSO containing 0.1 M $^nBu_4NPF_6$). Measurements were conducted under an inert atmosphere of Ar gas at room temperature using 0.1 M $^nBu_4NPF_6$ as the supporting electrolyte in anhydrous DMSO. The concentration of Cu(II) complexes was 5×10^{-3} M. Quasi-reversible behavior was observed and half-wave potentials ($E^{\circ\prime}$) were found to be independent of scan rate between 1 and 100 mV s^{-1}. Experiments were performed at a scan rate of 20 mV s^{-1} and referenced to a ferrocene/ferrocenium internal standard (FeCp$_2^{+/0}$) which exhibits $E^{\circ\prime} = +0.68$ V vs NHE in DMSO.[69] All $E^{\circ\prime}$ are reported vs NHE.

Stopped-Flow Measurements. Stopped-flow kinetic measurements were performed on OLIS RSM 1000 spectrophotometer which has a 2−3 millisecond dead-time. The drive syringes and observation cell were thermostated to +20 °C using a recirculating water bath (ThermoHaake K20). Experiments were performed by 1:1 mixing of reagents with initial concentrations of 0.02, 0.21, and 2.1 mM. Measurements were conducted in multi- and single-wavelength modes. The rate of $Cu^{I}(TEPA)$ appearance was monitored at $\lambda_{max} = 345$ nm for the reactions of $Cu^{II}(TEPA)$ and $Cu^{II}N_3(TEPA)$. The rate of $Cu^{II}N_3(TMPA)$ disappearance was monitored at $\lambda_{max} = 412$ nm. All of the reactions proceeded to near completion within the mixing time of the instrument.

Low-temperature stopped-flow experiments at -57 °C and -80 °C were conducted using a Hi-Tech Scientific stopped-flow system. Mixing was performed through two stainless steel coils, lined with Teflon. One reservoir contained the copper reactants while the other contained $O_2^{\bullet-}$,
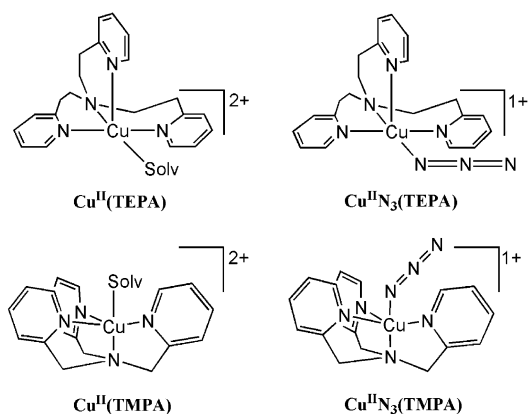

Figure 2. Structures and abbreviations of copper(II) complexes.

O_2, or mixtures thereof. O_2 solutions of desired concentration were prepared by purging solvents with O_2/Ar gas mixtures created with a MultiGas Controller 647C (MKS Instruments). The mixing chamber was immersed in an ethanol bath cooled by liquid N_2 evaporation for low-temperature measurements. The temperature was measured using a Pt resistance thermocouple and maintained to ±0.1 °C using a temperature-controlled thyristor unit (Hi-Tech). Data acquisition was performed using the Spectralys software (J & M).

Results

I. Description of Reactions. The structures of the copper(II) complexes and abbreviations used to refer to them are given in Figure 2. All of the complexes except for $Cu^{II}N_3(TEPA)$ have been shown by X-ray crystallography to adopt 5-coordinate geometries.[60,61,70−72] Both copper(II) TEPA complexes are expected to exhibit a square pyramidal geometry by analogy with others having H_2O and 1-methylimidazole[60,71] as well as anions such as NO$_3^-$, Cl$^-$ and acetate as the fifth ligands.[61,71,72] On the basis of these structures, N$_3^-$ and solvent are expected to coordinate at the base of the square pyramid with one elongated $Cu-N_{Py}$ bond coordinated to the apical site. $Cu^{I}(TEPA)$ crystallized from noncoordinating solvents is pseudo-tetrahedral and distorted toward trigonal pyramidal geometry.[60] In contrast, both copper(I) and copper(II) complexes of TMPA are trigonal bipyramidal with solvent (CH$_3$CN) or an anion (Cl$^-$, N$_3^-$, NO$_2^-$, NCS$^-$) in the case of copper(II) occupying an apical site.[61,62,70,73] These structural differences may influence the barriers to redox reactions as well as the energies of intermediates formed upon reacting copper(I) with O_2 and copper(II) with $O_2^{\bullet-}$.

All of the copper(II) complexes react rapidly with $O_2^{\bullet-}$ at 22 °C in DMSO, where the radical anion is both a powerful reductant and a nucleophile. The related copper(I) complexes and O_2 are formed as products in yields that depend on the initial concentrations of the reactants. When substoichiometric amounts of $O_2^{\bullet-}$ are added to $Cu^{II}(TEPA)$, the yield of $Cu^{I}(TEPA)$ is 66 ± 5%. The reaction of $Cu^{II}N_3(TEPA)$ with $O_2^{\bullet-}$ also forms $Cu^{I}(TEPA)$ in 60 ± 7% yield indicating that the product is thermodynamically unstable with respect to loss of N$_3^-$. No reaction is observed between $Cu^{I}(TEPA)$ and O_2 under the

(69) Sawyer, D. T.; Sobkowiak, A.; Roberts, J. L., Jr. *Electrochemistry for Chemists*; Wiley: New York, 1995.

(70) Mukhopadhyay, U.; Bernal, I.; Massoud, S. S.; Mautner, F. A. *Inorg. Chim. Acta* **2004**, *357*, 3673.

(71) Alilou, E. H.; Hallaoui, A. E.; Ghadraoui, H. E.; Giorgi, M.; Pierrot, M.; Reglier, M. *Acta Crystallogr. Sect. C* **1997**, *53*, 559.
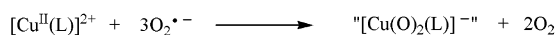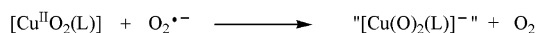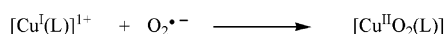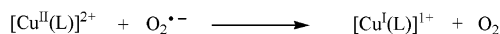
(72) Karlin, K. D.; Dahlstrom, P. L.; Hayes, J. C.; Simon, R. A.; Zubieta, J. *Cryst. Struct. Comm.* **1982**, *11*, 907.

(73) Lim, B. S.; Holm, R. H. *Inorg. Chem.* **1998**, *37*, 4898.

Table 1. Yields of O$_2$ Based on Copper(I) and Copper(II) Complexes in 10:1 DMSO/DMF at 22 °C

entry	oxidant	1 eq. O$_2^{•-}$	2 eq. O$_2^{•-}$	≥ 3 eq. O$_2^{•-}$
1	**Cu^{II}(TEPA)**	68 ± 4%	133 ± 1%	192 ± 32%[a]
2	**Cu^{II}N$_3$(TEPA)**	73 ± 1%	147 ± 2%	201 ± 18%[a]
3	**Cu^{II}(TMPA)**	72 ± 3%	142 ± 1%	189 ± 23%[a]
4	**Cu^{II}N$_3$(TMPA)**	72 ± 1%	142 ± 3%	193 ± 33%[a]
5	**Cu^{I}(TEPA)**	53 ± 6%		91 ± 9%[b]
6	**Cu^{I}(TMPA)**	51 ± 6%		115 ± 19%[b]

[a] 3–8 equiv. [b] 2–6 equiv.

$$[Cu^{II}(L)]^{2+} + O_2^{•-} \longrightarrow [Cu^{I}(L)]^{1+} + O_2$$

$$[Cu^{I}(L)]^{1+} + O_2^{•-} \longrightarrow [Cu^{II}O_2(L)]$$

$$[Cu^{II}O_2(L)] + O_2^{•-} \longrightarrow \text{"}[Cu(O)_2(L)]^{-}\text{"} + O_2$$

$$[Cu^{II}(L)]^{2+} + 3O_2^{•-} \longrightarrow \text{"}[Cu(O)_2(L)]^{-}\text{"} + 2O_2$$

Figure 3. Reactions of copper(I) and copper(II) complexes with O$_2^{•-}$.

experimental conditions,[74] thus precluding this as an explanation of the lower than expected product yields. Yields of the **Cu^{II}(TMPA)** and **Cu^{II}N$_3$(TMPA)** reactions with O$_2^{•-}$ were analyzed using an alternative method to avoid the subsequent reactivity of the copper(I) products with O$_2$. The reactants were mixed 1:1 under dynamic vacuum while sweeping the solutions with He gas to remove the O$_2$ produced. Subsequent evaporation of the solvent and analysis of the remaining solids by ^{1}H NMR indicated formation of **Cu^{I}(TMPA)** in an average yield of 44 ± 13%.[75] Again, the thermodynamic product did not contain bound N$_3^-$.

The O$_2$ produced under the conditions described above was quantified by manometry. Measurements were relative to the reaction with the **Co^{III}(SMDPT)** standard which converts all of the O$_2^{•-}$ in solution to O$_2$ (see **Experimental Methods**). When the copper(II) complexes were reacted with O$_2^{•-}$ in a 1:1 ratio, the 68–73% yields of O$_2$ obtained were somewhat higher than the yields of copper(I) products quoted above (Table 1, Entries 1–4). Increasing the ratio to 2:1, O$_2^{•-}$ to copper(II) complex, caused the yield of O$_2$ to increase to 133–147%. For the 3:1 reaction, a yield of 189–201% was obtained. No further increase in the O$_2$ yield was observed when 3–8 equivalents of O$_2^{•-}$ were reacted per mol of copper(II) complex.

The increase in O$_2$ yield, in direct proportion to the increased ratio of O$_2^{•-}$ to copper(II) complex, is due to the subsequent reactions of **Cu^{I}(TEPA)** or **Cu^{I}(TMPA)**. The stoichiometry of these reactions was determined by quantifying the O$_2$ formed at varying ratios of O$_2^{•-}$ to the copper(I) complexes (Table 1, Entries 5 and 6). The 1:1 reactions resulted in yields of 51–53% indicating that two equivalents of O$_2^{•-}$ were consumed per equivalent of O$_2$ formed. With 2 to 6 equivalents of O$_2^{•-}$ per mol of copper(I) complex, the yield increased to 91–115%. The results are consistent with the scheme in Figure 3 wherein three equivalents of O$_2^{•-}$ react with a single copper(II) complex

Table 2. Thermodynamics for the Oxidation of O$_2^{•-}$ to O$_2$ by Copper(II) Complexes

	$E°'$ (V vs NHE)	$\Delta G°$ (kcal mol^{-1})	w_P–w_R (kcal mol^{-1})	$\Delta G°'$ (kcal mol^{-1})
Cu^{II}(TEPA)	+0.52[a]	−24.4	+5.5	−18.9
Cu^{II}N$_3$(TEPA)	+0.38[b]	−21.2	+2.8	−18.4
Cu^{II}(TMPA)	−0.05[c]	−11.3	+5.5	−5.8
Cu^{II}N$_3$(TMPA)	−0.15[d]	−9.0	+2.8	−6.2

[a] $E_a - E_c$ = 0.41 V and $i_{p,a}/i_{p,c}$ = 0.74. [b] $E_a - E_c$ = 0.27 V, $i_{p,a}/i_{p,c}$ = 0.82. [c] $E_a - E_c$ = 96 mV and $i_{p,a}/i_{p,c}$ = 0.95. [d] $E_a - E_c$ = 92 mV and $i_{p,a}/i_{p,c}$ = 0.90.

and are converted to two equivalents of O$_2$ and an as yet unidentified copper species.

Attempts to characterize the final copper-containing product from reactions of copper(I) or copper(II) complexes with excess O$_2^{•-}$ have thus far been unsuccessful. ^{1}H NMR analysis indicates a diamagnetic compound is formed and complete mass balance of the reaction.[76] The product mixture does not appear to contain H$_2$O$_2$ or a copper product with an intact O–O bond. This conclusion is based on the absence of detectable levels of H$_2$O$_2$ upon hydrolysis and assay with horseradish peroxidase and diammonium salt of 2,2′-azino-bis(3-ethylbenzothiazoline-6-sulfonate) (ABTS).[77]

II. Thermodynamic Analysis. Cyclic voltammetry experiments (DMSO, 0.1 M ^{n}Bu$_4$PF$_6$, 22 °C) revealed a single wave corresponding to the Cu$^{II/I}$ redox couples (Table 2). The chemical reversibility was somewhat poorer for the more oxidizing TEPA complexes than for the TMPA complexes. The overall free energies ($\Delta G°$) corresponding to O$_2^{•-}$ oxidation via the first reaction in Figure 3 were estimated from half-wave potentials ($E°'$) of the copper complexes and $E°'$ = −0.54 V for O$_2^{0/-}$ in DMSO.[69] The equation used was: $\Delta G° = nF\Delta E°'$, where n is the number of electrons transferred, and F is Faraday's constant (23.06 kcal mol^{-1} V^{-1}).

Oxidations of O$_2^{•-}$ by **Cu^{II}(TEPA)** and **Cu^{II}N$_3$(TEPA)** are highly exoergic with $\Delta G°$ of −24.4 and −21.2 kcal mol^{-1}. The reactions of **Cu^{II}(TMPA)** and **Cu^{II}N$_3$(TMPA)** are less favorable with $\Delta G°$ of −11.3 kcal mol^{-1} and −9.0 kcal mol^{-1}. The derived $\Delta\Delta G°$ of 12–13 kcal mol^{-1} reflects the much greater stabilization of the copper(I) state in the TEPA ligand framework.[78] The large difference provides an explanation as to why **Cu^{I}(TMPA)** is highly reactive with O$_2$ whereas **Cu^{I}(TEPA)** is completely inert to O$_2$ in polar organic solvents from 20 to −80 °C. Within each ligand environment, coordination of N$_3^-$ resulted in a negative shift in redox potential amounting to $\Delta\Delta G°$ = 2–3 kcal mol^{-1}. A larger difference in O$_2^{•-}$ binding energy, approaching 13 kcal mol^{-1}, is expected based on the Cu$^{II/I}$ redox potentials.[79]

Analysis of the electrochemical potentials gives the net driving-force for the bimolecular reaction of copper(II) complexes and O$_2^{•-}$ to form the related copper(I) complexes and O$_2$. However, corrections must be applied for the electrostatic

(74) Schatz, M.; Becker, M.; Thaler, F.; Hampel, F.; Schindler, S.; Jacobson, R. R.; Tyeklar, Z.; Murthy, N. N.; Ghosh, P.; Chen, Q.; Zubieta, J.; Karlin, K. D. *Inorg. Chem.* **2001**, *40*, 2312.
(75) The yield of **Cu^{I}(TMPA)** was determined by ^{1}H NMR analysis of three independent samples prepared from crude reaction mixtures. See Supporting Information for details.
(76) A 3.5 × 10^{-2} M solution of **Cu^{II}(TEPA)** in DMSO-d_6 treated with excess KO$_2$ solubilized with 18-crown-6 (2.4 × 10^{-2} M) in DMSO-d_6 at room temperature reveals signals corresponding to **Cu^{I}(TEPA)** and three broad singlets. The latter occur at δ 8.60, 7.74, 7.27 ppm and integrate 1:1:2, respectively. The integrated intensities indicate the complete mass balance in the reaction suggesting the formation of a single diamagnetic product.
(77) Santagostini, L.; Gullotti, M.; Monzani, E.; Casella, L.; Dillinger, R.; Tuczek, F. *Chem. Eur. J.* **2000**, *6*, 519.
(78) Rorabacher, D. B. *Chem. Rev.* **2004**, *104*, 651.
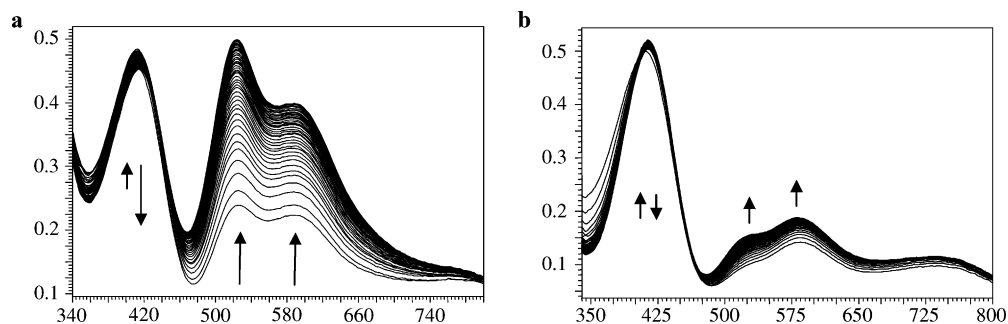(79) Taube, H. *Prog. Inorg. Chem.* **1986**, *34*, 607.

Figure 4. Time-dependent UV−vis spectra taken during the first 100 ms in 4:1 DMF:THF at −80 °C. Initial concentrations of reactants after mixing are as follows: (a) [$Cu^{II}(TMPA)$] = 5.5 × 10^{-4} M, [$O_2^{•-}$] = 1.25 × 10^{-4} M and (b) [$Cu^{I}(TMPA)$] = 1.25 × 10^{-4} M, [O_2] = 1.25 × 10^{-4} M.

attraction of oppositely charged reactants in order to evaluate the thermodynamics of the unimolecular electron transfer (ET) step. For this purpose, electrostatic work terms (w_R and w_P), which represent the free energies of interactions within a complex of the reactants or products, are calculated using a dielectric continuum model.[80]

In the most basic approach (eq 2), terms include the permittivity of vacuum constant (e^2 = 332.1 Å kcal mol^{-1}), the reactant or product charges (Z_1 and Z_2), the dielectric screening factor (f_{sf}), the static dielectric constant (D_s), which is 47.24 for DMSO,[81] and the internuclear distance (r_{12}). The close approach of $O_2^{•-}$ to the copper center is modeled by assuming r_{12} = 2.0 Å and the resulting f_{sf} = 0.80.[82] The former value is based on Cu−O distances in crystal structures of **$Cu^{II}(TEPA)$** with nitrate and acetate counterions.[71,72] The difference in electrostatic work terms (w_P-w_R) is then subtracted from $\Delta G°$ to obtain the effective driving-force for the uni-molecular redox step ($\Delta G°'$) (Table 2). It is important to note that covalent bonding between the reactants is not reflected in these work terms and a CuO_2 intermediate may be either more or less stable than the complexes held together only by electrostatics.[79]

$$w_R \text{ or } w_P = \frac{e^2 Z_1 Z_2 f_{sf}}{D_s r_{12}} \quad (2)$$

III. Detection of Intermediates. Stopped-flow spectro-photometric measurements at varying temperatures were undertaken to detect intermediates during $O_2^{•-}$ oxidation by copper(II) complexes. Rates were too fast to measure in DMSO at 20 °C, which is just above the freezing point of this solvent. Even one of the least thermodynamically favorable reactions involving **$Cu^{II}N_3(TMPA)$** (1 × 10^{-5} M) and $O_2^{•-}$ (1 × 10^{-5} M) had reached completion within the 3 millisecond mixing time of the stopped-flow instrument. A lower limit to the second-order rate constant of ≥1 × 10^8 $M^{-1}s^{-1}$ is, therefore, estimated under bimolecular conditions from k = $1/t_{1/2}[A]_0$; the reaction half-life ($t_{1/2}$) was ≤1 millisecond and each reactant was present at an initial concentration of $[A]_0$.

Low-temperature, stopped-flow experiments were performed in DMF (−57 °C) and in a 4:1 mixture of DMF/THF (−80 °C). 18-crown-6 ether was used to solubilize the KO_2 in both solvents. Although these experiments are not directly compa-rable to those at ambient temperature in DMSO, they provide insight to possible reaction intermediates. The 1:1 reaction of **$Cu^{II}(TEPA)$** (5.0 × 10^{-4} M) and $O_2^{•-}$ (5.0 × 10^{-4} M) at −57 °C was over within the spectrometer's mixing time as evidenced

by the lack of optical change and the absorbance corresponding to **$Cu^{I}(TEPA)$** present in 65 ± 8% yield. Under these condi-tions, a lower limit to the second-order rate constant of ≥2 × 10^6 $M^{-1}s^{-1}$ is estimated as described above. The reactions of **$Cu^{II}(TMPA)$** and **$Cu^{II}N_3(TMPA)$** with $O_2^{•-}$ were examined under similar conditions at −57 °C and at −80 °C using a 3−4-fold excess of the copper complexes relative to $O_2^{•-}$ in order to minimize competing side reactions. The spectral data obtained at both low temperatures were similar. Within 3 milliseconds of mixing **$Cu^{II}(TMPA)$** and $O_2^{•-}$ at −80 °C, an intermediate is detected that is spectroscopically similar to a 1:1 Cu(TMPA):O_2 adduct previously observed upon reacting **$Cu^{I}(TMPA)$** and O_2 in propionitrile and in THF.[32,33,35] The manner in which O_2 is coordinated to the copper center in this intermediate has not been established.[83] However, an end-on superoxo structure has been invoked to explain the reactivity toward a second equiv. of **$Cu^{I}(TMPA)$** and the formation of the trans-μ-1,2-peroxo compound: [Cu(TMPA)]$_2O_2$.[84]

Spectroscopic data from the reaction of **$Cu^{II}(TMPA)$** and $O_2^{•-}$ are strikingly similar to those obtained upon reacting **$Cu^{I}(TMPA)$** and O_2 under the analogous conditions; yet formation of the dicopper peroxo product occurs on different time scales (Figure 4). The 1:1 Cu(TMPA):O_2 intermediate has prominent absorbance bands at 412, 580, and 765 nm and decays concomitant with the appearance of absorbance bands at 525 and 600 nm which have been assigned to [Cu(TMPA)]$_2O_2$.[84]

Within the dead-time of the stopped-flow, the reaction of **$Cu^{II}(TMPA)$** (5.5 × 10^{-4} M) and $O_2^{•-}$ (1.25 × 10^{-4} M) gives the intermediate 1:1 Cu(TMPA):O_2 adduct and [Cu(TMPA)]$_2O_2$ in yields of 75 ± 8% and 11 ± 5%, respectively (Figure 4a). The concentration of [Cu(TMPA)]$_2O_2$ increases to 32 ± 5% over the course of 100 milliseconds. The formation of the dicopper peroxo product is inhibited by added O_2 (5.4 × 10^{-3} M) consistent with an earlier step involving dissociation of the 1:1 Cu(TMPA):O_2 to form **$Cu^{I}(TMPA)$**. As discussed above (**Results, I.**), the rapid reaction of **$Cu^{I}(TMPA)$** with $O_2^{•-}$ is expected to give a mononuclear copper(II) peroxo species,[85] which could then react with a second equivalent of **$Cu^{II}(TMPA)$** to generate the final product.

(80) Sutin, N. *Prog. Inorg. Chem.* **1983**, *30*, 441.
(81) Lide, D. R., Ed. *CRC Handbook of Chemistry and Physics*, 84th ed.; CRC Press: Boca Raton, FL, 2003.
(82) Here f_{sf} = 1/[1 + $r_{12}(8\pi e^2\mu/10^{27}D_s k_B T)^{1/2}$] and r_{12} = 2 Å; e^2 = 332.0637 kcal Å mol^{-1}; μ = 0.1 mol L^{-1}; D_s = 47.24; k_B = 3.2998 × 10^{-27} kcal K^{-1}; T = 298.15 K.
(83) Karlin, K. D.; Kaderli, S.; Zueberbuehler, A. D. *Acc. Chem. Res.* **1997**, *30*, 139.
(84) Jacobson, R. R.; Tyeklar, Z.; Farooq, A.; Karlin, K. D.; Liu, S.; Zubieta, J. *J. Am. Chem. Soc.* **1988**, *110*, 3690.
(85) Burstyn, J. N.; Roe, J. A.; Miksztal, A. R.; Shaevitz, B. A.; Lang, G.; Valentine, J. S. *J. Am. Chem. Soc.* **1988**, *110*, 1382.
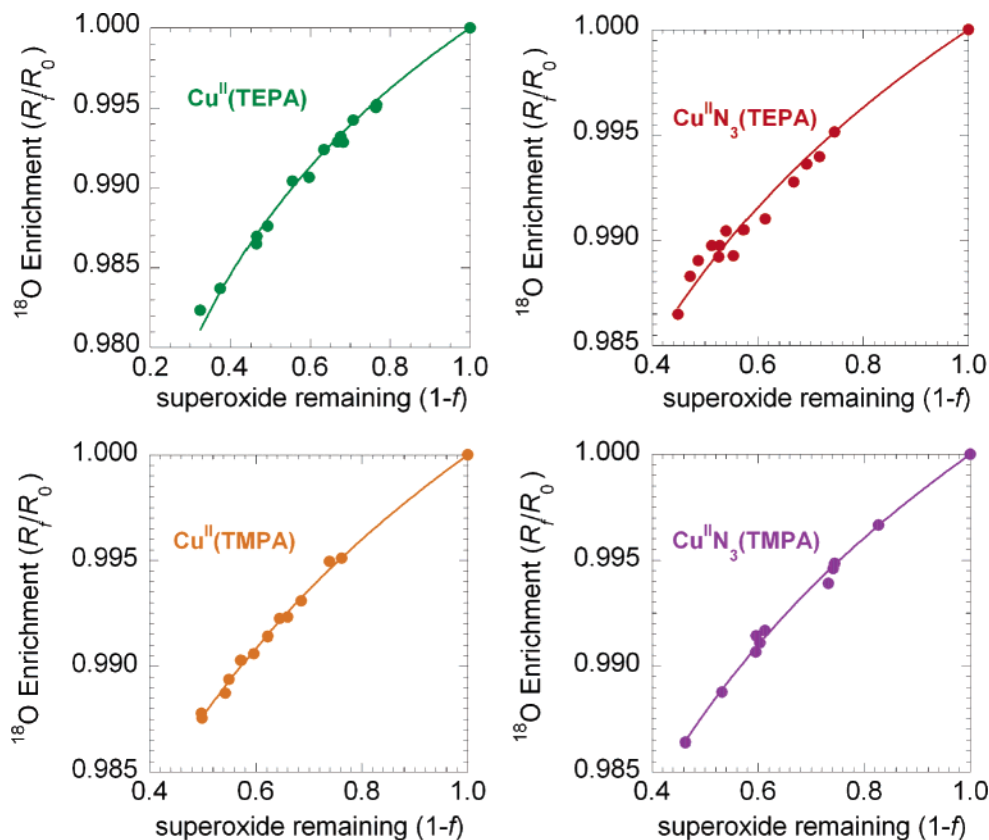
Figure 5. Isotope fractionation during reactions of copper(II) complexes with excess $O_2^{\bullet-}$ (22 °C, 10:1 DMSO:DMF).

The reaction of **Cu^I(TMPA)** (1.25×10^{-4} M) and O_2 (1.25×10^{-4} M) forms the 1:1 Cu(TMPA):O_2 intermediate in $96 \pm 7\%$ yield. However, unlike the reaction of **Cu^{II}(TMPA)** and $O_2^{\bullet-}$, the concentration of the intermediate changes by $\leq 3 \pm 5\%$ over 100 milliseconds (Figure 4b). The much slower buildup of the [Cu(TMPA)]$_2$O$_2$ product, as well as the independence of rate on added **Cu^{II}(TMPA)** (5.0×10^{-4} M), indicates a different mechanism than described above. This mechanism most likely involves the coordination of **Cu^I(TMPA)** to the 1:1 Cu(TMPA): O_2 adduct.[33,35]

The copper(I) and copper(II) complexes appear to react through monomeric structures. This point is raised because a pyridyl-bridged copper(I) dimer [Cu^I(TMPA)]$_2$ has been assigned as the dominant species in acetone solutions prepared from **Cu^I(TMPA)**. Reaction of [Cu^I(TMPA)]$_2$ with O_2 in this solvent initially gives a 2:1 Cu(TMPA):O_2 intermediate in ~50% yield based on copper.[33] ^{1}H NMR analysis of **Cu^I(TMPA)** in DMF at -57 °C reveals some degree of aggregation possibly to [Cu^I(TMPA)]$_2$.[33] However, the high yield ($96 \pm 7\%$) of the 1:1 Cu(TMPA):O_2 intermediate obtained from **Cu^I(TMPA)** and O_2 in DMF and DMF:THF mixtures allows the reaction through the dimeric structure to be excluded.

The low-temperature, stopped-flow results are consistent with, although do not prove, that the same 1:1 Cu(TMPA):O_2 intermediate is the primary product of the reaction between **Cu^{II}(TMPA)** and $O_2^{\bullet-}$ as well as the reaction between **Cu^I(TMPA)** and O_2. The possibility that the 1:1 Cu(TMPA): O_2 adduct is a secondary product of one or both of these reactions cannot be excluded on the basis of our stopped-flow measurements because the rate of the intermediate's formation

is too fast to be monitored. If the 1:1 Cu(TMPA):O_2 adduct were formed as a secondary product, then the reaction would involve initial outer-sphere electron transfer followed by an association step. This mechanism is addressed (below) in the context of competitive kinetic isotope effect measurements.

IV. Competitive Oxygen Kinetic Isotope Effects. Competitive ^{18}O KIEs were determined from the fractionation of oxygen isotopes, i.e., the change in ^{18}O/^{16}O during the oxidation of $O_2^{\bullet-}$ to O_2 by the various copper complexes. Because the reactions are extremely rapid, measurements were performed using excess $O_2^{\bullet-}$ and varying sub-stoichiometric amounts of copper rather than in a time dependent manner. By virtue of being a competitive measurement, the isotope effect derives from the second-order rate constants for the disappearance of light ^{16}O$-$^{16}O$^{\bullet-}$ and heavy ^{18}O$-$^{16}O$^{\bullet-}$ ($^{16,16}k/^{18,16}k$). The ^{18}O KIE is expressed as a ratio of ratios according to Eq 3 which contains terms for the initial ^{18}O/^{16}O in $O_2^{\bullet-}$ at time 0 (R_0) and the ^{18}O/ ^{16}O of $O_2^{\bullet-}$ remaining in the solution (R_f) at a specific fractional consumption of $O_2^{\bullet-}$ (f). R_0 was determined by direct measurement using the standard reaction of **Co^{III}(SMDPT)** (see Experimental Methods). R_f was determined from the ^{18}O/^{16}O of the O_2 produced (R_{O_2}) at a specific fractional yield (f) using eq 4.

$$\frac{R_f}{R_0} = (1 - f)^{1/(^{16,16}k/^{18,16}k)-1} \tag{3}$$

$$R_0 = R_f(1 - f) + R_{O_2}(f) \tag{4}$$

Isotope fractionation plots for the oxidation of $O_2^{\bullet-}$ by copper(II) complexes are shown in Figure 5. The data are well-fitted by

Table 3. Competitive ^{18}O KIEs on Reactions of $O_2^{\bullet-}$ with Copper(I) and Copper(II) Complexes

isotope effect[a] $(^{16,16}k/^{18,16}k)_I$	$Cu^I(TEPA)$ 0.9808 ± 0.0018		$Cu^I(TMPA)$ 0.9818 ± 0.0014	
	$Cu^{II}(TEPA)$	$Cu^{II}N_3(TEPA)$	$Cu^{II}(TMPA)$	$Cu^{II}N_3(TMPA)$
$(^{16,16}k/^{18,16}k)_{net}$	0.9829 ± 0.0017	0.9834 ± 0.0023	0.9824 ± 0.0011	0.9825 ± 0.0017
$(^{16,16}k/^{18,16}k)_{II}$	0.9871 ± 0.0062	0.9886 ± 0.0078	0.9836 ± 0.0043	0.9839 ± 0.0058

[a] See text for description of terms.

eq 3 indicating that neither the mechanism nor the rate-determining step which gives rise to the ^{18}O KIE changes as the reaction progresses. In addition, the ^{18}O KIE was found to be independent of the starting molar ratio of the $O_2^{\bullet-}$ to the copper(II) complexes from 3:1 to 8:1 as well as the addition of 18-crown-6 ether which destabilizes the $K^+O_2^{\bullet-}$ tight ion pair.

Although small in magnitude, the competitive ^{18}O KIEs are determined very precisely through 10−15 independent measurements. To be conservative, errors are reported as two standard deviations about the mean calculated value rather than the much smaller 2σ error from the nonlinear curve-fitted data. Although the isotope ratio mass spectrometric analysis is typically precise to ± 0.0002, slightly larger errors are indicated by the $R_0 =$ 1.01733 (± 0.00051) vs standard mean ocean water (SMOW), which was determined for commercial (nonenriched) KO_2 by 22 independent measurements. This error reflects the reproducibility of the reaction chemistry as well as the experimental manipulations which include a combustion step (see Experimental Methods).

All of the reactions are characterized by a decrease in the '^{18}O enrichment' of the unreacted $O_2^{\bullet-}$ as the fractional conversion to O_2 increases (Figure 5). This observation indicates that the heavier $^{18,16}O_2^{\bullet-}$ reacts faster than the lighter $^{16,16}O_2^{\bullet-}$ and, therefore, an inverse (<1) ^{18}O KIE. Since the experiments were performed in the presence of excess $O_2^{\bullet-}$, contributions from the follow-up reactions of $Cu^I(TEPA)$ and $Cu^I(TMPA)$ are also considered. The KIEs on these reactions were determined using the same procedure outlined for the copper(II) complexes. The data are well-described by eqs 3 and 4 (See Supporting Information) again indicating that the isotopically sensitive step does not change as the reaction progresses.

The ^{18}O KIEs on the reactions of the copper(II) complexes with $O_2^{\bullet-}$ to form the related copper(I) complexes and O_2 are designated: $(^{16,16}k/^{18,16}k)_{II}$. These values were estimated using Eq 5 where $(^{16,16}k/^{18,16}k)_{net}$ is the observed isotope effect starting with $Cu^{II}(TEPA)$, $Cu^{II}N_3(TEPA)$, $Cu^{II}(TMPA)$, or $Cu^{II}N_3$-$(TMPA)$ and $(^{16,16}k/^{18,16}k)_I$ is the observed isotope effect starting with $Cu^I(TEPA)$ or $Cu^I(TMPA)$ (Table 3). The equation accounts for the $3O_2^{\bullet-}$ to $2O_2$ stoichiometry determined from the reaction yields (cf. Figure 3). The derived $(^{16,16}k/^{18,16}k)_{II}$: $Cu^{II}(TEPA) = 0.9871 \pm 0.0062$, $Cu^{II}N_3(TEPA) = 0.9886 \pm$ 0.0078, $Cu^{II}(TMPA) = 0.9836 \pm 0.0043$ and $Cu^{II}N_3(TMPA)$ = 0.9839 ± 0.0058 are the same within the 2σ limits of propagated error. Importantly, the measured $(^{16,16}k/^{18,16}k)_I$ are virtually identical (Table 3). Therefore, any deviation from theoretical relationships in eqs 3−5 has no bearing on the relative correction to $(^{16,16}k/^{18,16}k)_{net}$ and the major conclusion that the $(^{16,16}k/^{18,16}k)_{II}$ are indistinguishable for the reactions of the different copper(II) complexes.

$$(^{16,16}k/^{18,16}k)_{II} = 3(^{16,16}k/^{18,16}k)_{net} - 2\,(^{16,16}k/^{18,16}k)_I \quad (5)$$

Discussion

Reactions of $O_2^{\bullet-}$ with labile transition metal complexes frequently occur at rates that approach the diffusion limit.[16,17] Therefore, it is not surprising that the copper(II) complexes studied here, which have open or easily substituted coordination sites, react at rates too fast to be studied using low-temperature stopped-flow spectrophotometry. The following discussion will show how competitive ^{18}O KIEs, together with an analysis of the reaction thermodynamics, provide unique insight to the mechanisms and barriers associated with transition-metal mediated $O_2^{\bullet-}$ oxidations. In addition, the characterization of activated oxygen intermediates through comparisons of measured ^{18}O isotope effects to theoretically calculated values will be described.

I. Mechanism of Superoxide Oxidation. There are at least four mechanisms which can be envisioned for the one-electron oxidation of $O_2^{\bullet-}$ by copper(II) complexes to give O_2 and the related copper(I) species: (i) outer-sphere electron transfer (ET), (ii) single-step, inner-sphere ET, (iii) multistep, inner-sphere ET where the formation of a bound intermediate is rate-limiting, and (iv) multistep, inner-sphere ET where the dissociation of a bound intermediate is rate-limiting.

The simplest mechanism involves ET in a single-step. In the context of Marcus theory, the transition state for an outer-sphere ET reaction is an activated nuclear configuration of the reactants and the surrounding solvent. In this configuration, there is no formal bonding and only weak electronic coupling between the reactants. In contrast, inner-sphere ET involves a transition state with a bond between the reactants. With respect to the reactions of interest, the rate-determining step for an inner-sphere ET might involve simple binding of $O_2^{\bullet-}$ to Cu^{II}, the dissociation of O_2 from a CuO_2 intermediate, or a concerted reaction in which both processes occur at the same time.

In practice, it is often difficult to distinguish inner-sphere from outer-sphere ET reactions of O_2, although Marcus Theory has been used.[86,87] According to the Marcus Cross Relation (eq 6)[88] the rate constant (k_{12}) for an outer-sphere ET can be expressed in terms of the equilibrium constant (K_{12}') derived from $\Delta G^{\circ\prime}$, a frequency factor (f_{12}),[89] and self-exchange rate constants (k_{11} and k_{22}) for two degenerate reactions generalized as: $*A + B \rightarrow *B + A$; the $*$ designates the initial site of the electron.

$$k_{12} = \sqrt{k_{11} \times k_{22} \times K_{12}' \times f_{12}} \quad (6)$$

The Cross Relation has been noted to fail when rates of outer-sphere ET approach the diffusion limit and when reactions occur

(86) Zahir, K.; Espenson, J. H.; Bakac, A. *J. Am. Chem. Soc.* **1988**, *110* (0), 5059.
(87) Stanbury, D. M.; Haas, O.; Taube, H. *Inorg. Chem.* **1980**, *19*, 518.
(88) Marcus, R. A.; Sutin, N. *Biochim. Biophys. Acta* **1985**, *811*, 265.
(89) $\ln(f_{12}) = (\ln K_{12}')^2/4[\ln(k_{11}k_{22}/Z^2) + (w_{11} + w_{22})/RT]$; w_{11} and w_{22} correspond to the formation of the precursor complex in the self-exchange reactions and $Z = 10^{11}$ M^{-1} s^{-1}.

by inner-sphere ET.[90] For one of the least thermodynamically favorable oxidations of $O_2^{•-}$ by $Cu^{II}N_3(TMPA)$, a value of $k_{12} = 2.4 \times 10^4$ $M^{-1}s^{-1}$ is calculated using aqueous self-exchange rate constants: $k_{11} = 4.5 \times 10^2$ $M^{-1}s^{-1}$ for $O_2 + O_2^{•-}$[91] and $k_{22} = 70$ $M^{-1}s^{-1}$ for $Cu^{II}(TMPA) + Cu^{I}(TMPA)$,[92] $K_{12}' = 3.5 \times 10^4$ (from $\Delta G°'$ in Table 2) and $f_{12} = 0.5$.[89] The use of aqueous self-exchange rate constants is expected to give a cross-reaction rate constant in DMSO to within an order of magnitude; this is based on calculated values for the electrostatic work terms and the reorganization energy.[93] The large (10^4-fold) discrepancy between the predicted rate constant and the observed $k_{12} \geq 1 \times 10^8$ $M^{-1}s^{-1}$ indicates that the reaction does not occur by an outer-sphere ET. However, this conclusion is not so compelling in the case of $Cu^{II}(TEPA)$ for which $k_{12} = 1.8 \times 10^7$ $M^{-1}s^{-1}$ is calculated and $k_{12} > 1 \times 10^8$ $M^{-1}s^{-1}$ is observed.

II. Isotope Effects on Outer-Sphere Electron Transfer. Heavy atom KIEs on outer-sphere ET reactions originate largely from the reorganization of isotopic bonds upon converting the reactant into the product state. This contribution to the inner-shell reorganization free energy (λ_i) can be formulated either semiclassically or quantum mechanically. Within the semi-classical limit, the isotope effect arises from an over-the-barrier transition and the influence of zero point energy differences as well as the thermal populations of excited vibrational states. In the quantum mechanical limit, the isotope effect arises from mass-dependent Franck–Condon factors which reflect a through-the-barrier transition due to nuclear tunneling.

In both the semiclassical and quantum mechanical limits, the reaction thermodynamics is expected to influence the KIEs.[94–98] Semiclassically, $\Delta G°'$ dictates the position of the isotope-dependent barrier defined by the intersection of the reactant and product surfaces. In this view, a normal KIE arises when the force constant characterizing the product is less than that for the reactant; whereas an inverse KIE arises when the force constant of the product is greater than that of the reactant. Quantum mechanically, $\Delta G°'$ modulates the KIE through the isotope-dependent overlap of vibrational wave functions associated with the reactant and product states. When the $\Delta G°'$ is very favorable, vibrational states of the reactant can overlap with excited vibrational states of the product. It follows that a higher density of states associated with the heavy isotope relative to light one can cause the KIE to be inverse despite the invariably normal (> 1) contributions from Franck–Condon factors.[96,99]

The ^{18}O KIEs measured for $O_2^{•-}$ oxidations are inverse and fall within a narrow range from 0.9836 ± 0.0043 to $0.9886 \pm$

0.0078. This small range is surprising given the large (ca. 15 kcal mol^{-1}) variation in the reaction driving-forces. These results are in contrast to others in the literature corresponding to outer-sphere ET reactions. Gould and Farid reported $k_H/k_D = 1.25 \pm 0.04$ and 1.30 ± 0.03 for the highly exergonic ($\Delta G° = -57.7$ kcal mol^{-1}) ET reactions in acetonitrile: $TCA^{•-}$ (TCA = 2,6,9,10-tetracyanoanthracene) + toluene$^{•+}$ (d$_0$ vs d$_8$) and $TCA^{•-}$ + p-xylene$^{•+}$ (d$_0$ vs d$_{10}$).[100] Upon changing the $\Delta G°$ to -27.9 kcal mol^{-1}, by substituting ClO (chlorine oxide) in place of TCA, Simon and co-workers found k_H/k_D was dramatically decreased to 1.0 ± 0.1 and to 0.67 ± 0.1 for the respective hydrocarbons.[95,96]

In a more closely related study by McLendon and co-workers, the $k_{H_2^{16}O}/k_{H_2^{18}O}$ upon outer-sphere ET oxidation of $Fe(H_2O)_6^{2+}$ to $Fe(H_2O)_6^{3+}$ was measured. The ^{18}O KIEs were found to decrease from 1.08 ± 0.01 to 1.04 ± 0.01 as the driving-force changed from $\Delta G° = -11.5$ kcal mol^{-1} to $\Delta G° = -17.3$ kcal mol^{-1}.[97] Although the range of driving-forces is comparable to the range in present study, the ^{18}O KIEs are normal (>1) and vary significantly by $\sim 4\%$, compared to 0.5% in the present work. In addition, the conversion of $O_2^{•-}$ to O_2 and the conversion of $Fe(H_2O)_6^{2+}$ to $Fe(H_2O)_6^{3+}$ are both characterized by strengthening of the bond(s) (i.e., an increase in force constant) in the product states. The reactions of the iron complexes occur by outer-sphere ET and, because of the frequencies of the bonds involved, the ^{18}O KIEs are best explained within the quantum mechanical limit. We have previously shown that a quantum mechanical formalism can be used to predict normal ^{18}O KIEs on outer-sphere ET reductions of O_2 to $O_2^{•-}$ in the roughly thermoneutral regime.[94] In light of the results from earlier studies, the ^{18}O KIEs on $O_2^{•-}$ oxidation by copper(II) complexes, which are both inverse and independent of reaction driving-force, appear to be inconsistent with an outer-sphere ET mechanism.

O_2 binding reactions belong to a general class of inner-sphere ET reactions which may or may not involve the formation of intermediates with detectable lifetimes. We have previously reported large variations in ^{18}O KIEs, from 1.0273 to 1.0072, for concerted O_2 oxidative addition reactions that afford η^2-peroxo compounds from reduced late-transition metal complexes.[47] These reactions occur without any intermediates being formed. In addition, a trend of decreasing ^{18}O KIEs in response to the increased bimolecular rate constants for O_2 binding was observed. The trend has been attributed to variations in transition state structure in response to changing the reaction driving-force over an estimated -5.6 to -20 kcal mol^{-1}.[47,59] Because of the similar thermodynamics, a marked variation in transition state structure would be expected for the $O_2^{•-}$ oxidation reactions if they too were to occur by a one-step, inner-sphere ET pathway. Therefore, the lack of a discernible driving-force dependence of the ^{18}O KIEs in the present work argues against this type of mechanism.

III. Reaction Coordinate Analysis. Alternative mechanisms involve two steps where binding of $O_2^{•-}$ occurs first followed by the loss of O_2 from a CuO_2 intermediate. By definition, the competitive $(^{16,16}k/^{18,16}k)_{obs}$ reflects all elementary steps along the reaction coordinate from initial encounter of copper(II) complex with $O_2^{•-}$ up to and including the transition state for the first kinetically irreversible step. Therefore, the isotope effect

(90) Wherland, S. *Coord. Chem. Rev.* **1993**, *123*, 169.

(91) Lind, J.; Shen, X.; Merenyi, G.; Jonsson, B. O. *J. Am. Chem. Soc.* **1989**, *111*, 7654.

(92) Yandell, J. K. In *Copper Coordination Chemistry: Biochemical and Inorganic Perspective*; Karlin, K. D., Zubieta, J., Eds.; Adenine Press: Guilderland, NY, 1983; p 157.

(93) The overall reorganization (λ), the sum of inner (λ_{in}) and outer-shell (λ_{out}) contributions, is derived from bimolecular rate constants according to $k = 10^{11}M^{-1}s^{-1}\exp(-(\lambda/4k_BT)$. The calculated $\lambda_{in} = 15.9$ kcal mol^{-1} for $O_2/O_2^{•-}$ (ref 91) and $\lambda_{in} = 29.6$ kcal mol^{-1} for Cu^{II}/Cu^{I} (ref 92). The following static (D_s) and optical dielectric constants (D_o) were used to estimate the impact of changing λ_{out} upon k: $D_s = 47.24$, $D_o = 2.1883$ for DMSO and $D_s = 80.10$, $D_o = 1.7778$ for water (ref 81).

(94) Roth, J. P.; Wincek, R.; Nodet, G.; Edmondson, D. E.; McIntire, W. S.; Klinman, J. P. *J. Am. Chem. Soc.* **2004**, *126*, 15120.

(95) Doolen, R.; Simon, J. D.; Baldridge, K. K. *J. Phys. Chem.* **1995**, *99*, 13938.

(96) Doolen, R.; Simon, J. D. *J. Am. Chem. Soc.* **1994**, *116*, 1155.

(97) Guarr, T.; Buhks, E.; McLendon, G. *J. Am. Chem. Soc.* **1983**, *105*, 3763.

(98) Buhks, E.; Bixon, M.; Jortner, J. *J. Phys. Chem.* **1981**, *85*, 3763.

(99) Avouris, P.; Gelbart, W. M.; El-Sayed, M. A. *Chem. Rev.* **1977**, *77*, 793.

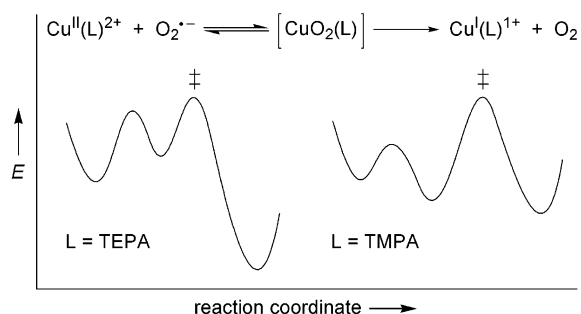(100) Gould, I. R.; Farid, S. *J. Am. Chem. Soc.* **1988**, *110*, 7883.

Figure 6. Reaction coordinate diagrams for the oxidation of $O_2^{\bullet-}$ by copper(II) complexes.

for a two-step reaction may be expressed as: $({}^{16,16}k/{}^{18,16}k)_{obs} = ({}^{16,16}K/{}^{18,16}K)_1({}^{16,16}k/{}^{18,16}k)_2$. The $({}^{16,16}K/{}^{18,16}K)_1 = ({}^{16,16}k/{}^{18,16}k)_1/({}^{16,16}k/{}^{18,16}k)_{-1}$ for the pre-equilibrium formation of a CuO_2 intermediate. The $({}^{16,16}k/{}^{18,16}k)_2$ corresponds to the first irreversible step where the intermediate is converted to products. If the initial binding step were kinetically irreversible, then regardless of the isotopic sensitivity of the second step, the following relationship would hold: $({}^{16,16}k/{}^{18,16}k)_{obs} = ({}^{16,16}k/{}^{18,16}k)_1$.

The indistinguishable ^{18}O KIEs observed for $O_2^{\bullet-}$ oxidation by the four copper(II) complexes imply that the same step is rate-determining in each of the reactions. It is unlikely that this is an initial $O_2^{\bullet-}$ binding step for the following reasons. (i) Indistinguishable ^{18}O KIEs are observed for the complexes with and without azide bound as a fifth ligand as well as complexes of dramatically different electrophilicity. The disparate energies of the putative CuO_2 intermediates should affect the position of the transition state and in turn the ^{18}O KIEs. (ii) The magnitude of the ^{18}O KIE is expected to be negligible for an electrostatic interaction with $O_2^{\bullet-}$ where electron transfer to copper(II) has not occurred to a significant extent (see below). Thus, on the grounds that the ^{18}O KIEs are significantly inverse as well as invariant to copper(II) complex coordination geometry, electrophilicity, and redox potential, a two step-mechanism involving rate-determining formation of a CuO_2 intermediate is considered improbable.

The remaining and favored mechanism involves formation of a CuO_2 intermediate prior to the rate-determining dissociation of O_2. Reaction coordinate diagrams corresponding to this mechanism for the different ligand complexes are shown in Figure 6; the ‡ designates the transition state which controls the disappearance of $O_2^{\bullet-}$ and formation of O_2. The stopped-flow studies suggest that the CuO_2 intermediate is stabilized relative to the separated reactants in the case of the TMPA complexes but destabilized for the TEPA complexes such that its concentration is undetectable. While the spectral data suggest that the intermediate is a $Cu(TMPA):O_2$ adduct, identical to that generated from **Cu^I(TMPA)** and O_2, an analysis of the kinetic mechanism has not been possible. The time scales of the low-temperature $O_2^{\bullet-}$ and the O_2 reactions are faster than the mixing-time of the stopped-flow instrument. However, the indistinguishable ^{18}O KIEs indicate that structurally similar CuO_2 intermediates are formed from the reactions of the copper(II) TEPA and TMPA complexes.

That the CuO_2 intermediate derived from **Cu^{II}(TEPA)** is thermodynamically less stable than the intermediate derived from **Cu^{II}(TMPA)** requires some discussion. The relative stability is likely affected by the redox potentials of the copper(II) centers as well as the ligand environment. Both of

these factors increase the contribution of the $Cu^I-O_2{}^0$ resonance form for the TEPA complexes but not so much for the TMPA complexes. Loss of electrostatic binding energy may be enough to destabilize the 1:1 $Cu(TEPA):O_2$ relative to the 1:1 $Cu(TMPA):O_2$ such that the former is unobservable in the low-temperature stopped-flow experiments,[101] yet not to the extent that the binding of $O_2^{\bullet-}$ is kinetically irreversible.

A two-step mechanism involving reversible formation of a CuO_2 intermediate is consistent with the invariance of the ^{18}O KIE over a wide range of ΔG°. This type of behavior would occur in the event that $({}^{16,16}k/{}^{18,16}k)_{obs}$ were largely determined by $({}^{16,16}K/{}^{18,16}K)_1$; i.e., if $({}^{16,16}k/{}^{18,16}k)_2$ were very small. By definition, $({}^{16,16}K/{}^{18,16}K)_1$ is independent of the reaction thermodynamics. This interpretation is analogous to those put forth in the organometallic chemistry literature to explain inverse primary H/D KIEs on alkane elimination from metal(alkyl)-(hydride) compounds via σ bonded intermediates.[102]

In the present experiments, the major change in force constant is believed to occur upon binding of $O_2^{\bullet-}$ in the first step, where some degree of internal ET results in strengthening of the $O-O$ bond and the formation of a $Cu-O$ bond. The observation of a small $({}^{16,16}k/{}^{18,16}k)_2$ would be consistent with an early transition state for the dissociation of O_2 requiring very little $O-O$ reorganization. This type of transition state structure is expected based on the favorable reaction driving-force. A negligible $({}^{16,16}k/{}^{18,16}k)_2$ could also result if a small inverse isotope effect on the elimination of O_2 were offset by a small normal isotope effect on the reaction coordinate frequency,[103] i.e., the bond that is lost upon converting a vibration to a translation in the transition state. In this view, a negligible isotope effect on the transition state for O_2 dissociation may occur even if the electron has only partially transferred prior to the rate-determining step. Regardless of the physical origin of the effect, the driving-force independence of the experimental results is most conveniently explained by $({}^{16,16}k/{}^{18,16}k)_{obs}$ being dominated by the $({}^{16,16}K/{}^{18,16}K)_1$ which describes the pre-equilibrium formation of the CuO_2 species.

IV. Calculation of Equilibrium ^{18}O Isotope Effects. The measured ^{18}O KIEs, taken to largely reflect pre-equilibrium formation of a CuO_2 intermediate, are consistent with our calculations of equilibrium isotope effects (EIEs). The ^{18}O EIEs were calculated for the binding of $O_2^{\bullet-}$ to copper(II) complexes and the formation of the proposed monomeric products in Table 4. These products were actually generated by reacting various copper(I) species with O_2. The approach, which employs Bigeleisen's formalism to calculate isotope effects, has been previously described.[104–107] The equations used are provided in Supporting Information.

Either two or three isotopically sensitive vibrations corresponding to the ν_{O-O} and ν_{Cu-O} of the copper complexes were considered along with the isotopic ν_{O-O} of $O_2^{\bullet-}$ and O_2. For

(101) This explanation may be extended to account for the lack of trapping of the putative $Cu(TEPA):O_2$ intermediate by copper(I) with formation of the dicopper peroxo product.
(102) Jones, W. D. *Acc. Chem. Res.* **2003**, *36*, 140.
(103) Melander, L.; Saunders: W. H., Jr. *Reaction Rates of Isotopic Molecules*; Wiley: New York, 1983.
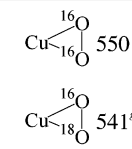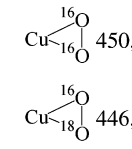(104) Slaughter, L. M.; Wolczanski, P. T.; Klinckman, T. R.; Cundari, T. R. *J. Am. Chem. Soc.* **2000**, *122*, 7953.
(105) Bender, B. R.; Kubas, G. J.; Jones, L. H.; Swanson, B. I.; Eckert, J.; Capps, K. B.; Hoff, C. D. *J. Am. Chem. Soc.* **1997**, *119*, 9179.
(106) Bender, B. R. *J. Am. Chem. Soc.* **1995**, *117*, 11239.
(107) Abu-Hasanayn, F.; Krogh-Jespersen, K.; Goldman, A. S. *J. Am. Chem. Soc.* **1993**, *115*, 8019.

Table 4. Calculated Equilibrium (^{18}O) Isotope Effects for the Oxidation of $O_2^{\bullet-}$ to O_2 and the Binding of $O_2^{\bullet-}$ to Copper(II) Complexes

Entry	Product (proposed structure)[a]	ν_{O-O}[b], cm^{-1}	ν_{Cu-O}[c], cm^{-1}	EIE[d]
1	O_2	$^{16}O-^{16}O$ 1556 $^{16}O-^{18}O$ 1512	—	0.968
2	$[Cu(L^{Me,Bn})(O_2)]^{+e}$ (end-on superoxo)	$^{16}O-^{16}O$ 1120 $^{16}O-^{18}O$ 1089[f]	Cu–$^{16}O^{16}O$ 474 Cu–$^{16}O^{18}O$ 474[g] Cu–$^{18}O^{16}O$ 454[g]	0.989
3	$[Cu(TMG_3tren)O_2]^{+h}$ (end-on superoxo)	$^{16}O-^{16}O$ 1117 $^{16}O-^{18}O$ 1089	Cu–$^{16}O^{16}O$ 438[i] Cu–$^{16}O^{18}O$ 437[i] Cu–$^{18}O^{16}O$ 421[i]	0.995
4	L3CuO$_2$[j] (side-on superoxo)	$^{16}O-^{16}O$ 1112 $^{16}O-^{18}O$ 1086[f]	Cu⟨$^{16}O/^{16}O$ 550 Cu⟨$^{16}O/^{18}O$ 541[g]	0.988-0.996[k]
5	$^2LCu(O_2)$[l] (side-on superoxo)	$^{16}O-^{16}O$ 1120 $^{16}O-^{18}O$ 1093	Cu⟨$^{16}O/^{16}O$ 450, 422 Cu⟨$^{16}O/^{18}O$ 446, 420	0.999
6	(1)Cu-β-diketiminate(O$_2$)[m] (side-on peroxo)	$^{16}O-^{16}O$ 968 $^{16}O-^{18}O$ 943	Unavailable[n]	0.994-1.005[o]
7	(2)Cu-β-diketiminate(O$_2$)[m] (side-on peroxo)	$^{16}O-^{16}O$ 961 $^{16}O-^{18}O$ 937	Unavailable[n]	0.995-1.006[o]

[a] All complexes were synthesized from copper(I) complexes and O₂ at low temperatures. Names and descriptors are in accord with the original literature: [Cu(TMG₃tren)O₂]$^+$ − tris[2-(tetramethylguanidino)ethyl]aminocopper superoxide, [Cu(L^{Me,Bn})(O₂)]$^+$ − tris(N-benzyl-*N*-methylaminoethyl)aminocopper superoxide, ^{2}LCu(O₂) − 2-[(4,7-diisopropyl)-1,4,7-triazacyclononylmethyl]-4,6-di-*tert*-butylphenoxy copper superoxide, L3CuO₂ − tris(3-*tert*-butyl-5-isopropyl-1-pyrazolyl)hydroboratocopper superoxide, (1)Cu-β-diketiminate(O₂) − *N,N′*-bis(2,6-diisopropylphenyl)-1,3-di-*tert*-butyl-β-diketiminatocopper superoxide, (2)Cu-β-diketiminate(O₂) − *N,N′*-bis(2,6-diisopropylphenyl)-1,3-dimethyl-β-diketiminatocopper superoxide. [b] The O−O stretch in free or complexed O₂. For free $O_2^{\bullet-}$: $^{16,16}\nu = 1064.8$ cm^{-1} and $^{18,16}\nu = 1034.8$ cm^{-1}.[110] [c] The Cu−O stretch for superoxo and peroxo complexes. For side-on complexes both the symmetric and asymmetric stretches are given. [d] The ^{18}O equilibrium isotope effect calculated using Bigeleisen's formalism.[110] [e] Ref.[111] [f] Estimated from $\nu_{^{18}O-^{16}O} = (\nu_{^{16}O-^{16}O} \times \nu_{^{18}O-^{18}O})^{1/2}$. [g] Estimated from the measured $\nu_{Cu-^{18}O-^{18}O}$. [h] Ref 39. [i] Computed value.[39] [j] Ref 112. [k] The more inverse EIE was estimated assuming that the isotope shift of the asymmetric ν_{Cu-O} was equal to that of the symmetric ν_{Cu-O}.[113] The less inverse EIE was estimated by neglecting isotope shift of the asymmetric ν_{Cu-O}. [l] Ref 114. [m] Ref 115. [n] Using either the frequencies and isotope shifts (given in parentheses): 462(−10) and 451(−9) cm^{-1} for the isostructural PtO₂(PPh₃)₂ (PPh₃ = triphenylphosphine) reported in ref 113 or those from entry 5. [o] The normal EIE was obtained using ν_{Cu-O} from entry 5 where coupling to Cu-ligand modes is apparent. The inverse EIE is a conservative lower limit which assumes idealized isotope shifts for pure symmetric and asymmetric ν_{Cu-O}.[113]

the proposed η^1-complexes, the low-frequency bend (δ_{Cu-O_2}) is reported to be relatively insensitive to isotope substitution[108] and was, therefore, neglected. In addition, calculations on the proposed end-on structures assumed equal populations of Cu−$^{18}O-^{16}O$ and Cu−$^{16}O-^{18}O$. This simplification can have the effect of making the calculated ^{18}O EIE slightly less inverse than the observed value. When stretching frequencies for the mixed-labeled isotopologues were unavailable, they were calculated from the data for the $^{16}O-^{16}O$ and $^{18}O-^{18}O$ containing species (entries 2 and 4 in Table 4). In some cases, it was necessary to assume values reported for isostructural compounds in the literature (entries 4, 6, and 7), and, therefore, a range of values is reported.

There is additional uncertainty associated with the assumption of pure O−O and Cu−O modes and the use of theoretical isotope shifts. When coupling to Cu−N or ligand C−N modes of the same symmetry and with similar force constants occurs, the stretching frequencies may be perturbed in such a way that the oxygen isotope shift is reduced relative to the theoretical value.[109] Depending on the degree of coupling, the ^{18}O EIEs may be significantly less inverse than in the absence of such interactions. This type of effect is apparent in the experimental frequencies in entry 5, where the isotope shifts of ν_{O-O} and ν_{Cu-O} are lower than the idealized, theoretical values.

The ^{18}O EIEs are formulated in terms of the change in force constant upon converting the reactant state to the product state.

(108) Odo, J.; Imai, H.; Kyuno, E.; Nakamoto, K. *J. Am. Chem. Soc.* **1988**, *110*, 742.

(109) For a leading reference, see: Kinsinger, C. R.; Gherman, B. F.; Gagliardi, L.; Cramer, C. J. *J. Biol. Inorg. Chem.* **2005**, *10*, 778.

As described in Results Section II, an increase results in an inverse isotope effect and a decrease results in a normal isotope effect. Several of the [18]O EIEs calculated for the formation of CuO_2 species from $O_2^{\bullet-}$ (Table 4) are inverse but significantly less so than the [18]O EIE of 0.968 associated with oxidizing $O_2^{\bullet-}$ to O_2. This result may be attributed to partial oxidation of $O_2^{\bullet-}$, due to the covalent sharing of an antibonding electron between copper and oxygen, and the strengthening of the O—O bond. In contrast, the partial reduction of bound $O_2^{\bullet-}$ populates an antibonding orbital which weakens the O—O bond.

The calculated [18]O EIEs for the proposed end-on superoxo (0.989−0.995), side-on superoxo (0.988−0.999) and side-on peroxo (0.994−1.006) structures reflect contributions from both internal ET and the appearance of new bonds between copper and oxygen. If the O—O force constant were the primary determinant of the EIE, then a trend from inverse to normal would be expected for a continuum from superoxo to peroxo type complexes.[31] The reason is that the formation of new Cu—O bonds can only increase the force constant of the product state and, therefore, contribute to an inverse EIE. For the peroxo-like (formally $Cu^{III}-O_2^{-II}$) structures, normal [18]O EIEs are estimated when, together, the isotope shifts of the symmetric and asymmetric ν_{Cu-O} total ≤ 11 cm^{-1}.[31] In contrast, the [18]O EIEs for the superoxo structures (formally $Cu^{II}-O_2^{-I}$) are invariably inverse, consistent with the synergetic effects of strengthening of the O—O bond (relative to free $O_2^{\bullet-}$) and forming new Cu—O bonds.

V. Structure of the Cu—O₂ Intermediate and Implications for Biological Systems. To shed light on the structures of the proposed CuO_2 intermediates formed from the reactions of copper(II) complexes and $O_2^{\bullet-}$, the $(^{16,16}k/^{18,16}k)_{obs}$ which approximate $(^{16,16}K/^{18,16}K)_1$ are compared to the [18]O EIEs calculated for structurally characterized compounds (Table 4). The $(^{16,16}k/^{18,16}k)_{obs}$ of 0.9836−0.9886 are consistent with that estimated for the proposed end-on superoxo complex: $[Cu(L^{Me,Bn})O_2]^+$.[111] While we stress that we cannot discern end-on from side-on superoxo structures based on the anticipated [18]O EIEs, it appears that a peroxo structure would have a value outside of the range observed. Furthermore, similar types of end-on superoxo structures for $[Cu(L^{Me,Bn})O_2]^+$ and $[Cu(TMPA)O_2]^+$ would be consistent with the complexes having the same overall charges and geometries enforced by the neutral tripodal ligands.

The thermodynamic relationship which exists between [18]O equilibrium isotope effects (EIEs), allows [18]O EIEs of 1.016 to 1.021 to be estimated in the direction of end-on O_2 binding to copper(I) complexes; this is accomplished by dividing the experimental values for $O_2^{\bullet-}$ binding copper(II) complexes by the theoretical [18]O EIE for converting $O_2^{\bullet-}$ to O_2 (Table 4). The values obtained are significantly larger than the [18]O EIEs of 1.0039−1.0046 reported for end-on O_2 binding to myoglobin and hemoglobin, the small size of which has been attributed to hydrogen bonding to the terminal oxygen in the O_2 carrier proteins.[110] We have calculated somewhat larger [18]O EIEs of 1.022−1.028 directly from the stretching frequencies of O_2 and the proposed end-on copper superoxo complexes (Table 4). The calculation further suggests that in favorable situations the [18]O

EIEs will be discernibly larger for forming side-on copper superoxo structures ($\sim$1.032) and larger still for forming side-on copper peroxo structures ($\sim$1.039) from copper(I) complexes and O_2.

It is interesting to compare the [18]O KIEs determined for O_2 reactions of enzymes with those calculated for reactions of biomimetic compounds. PHM and the structural homologue dopamine β-monooxygenase (DβM) exhibit competitive [18]O KIEs of 1.0212 ± 0.0018 and 1.0256 ± 0.0003, respectively.[52] In both of these enzymes, there is strong evidence of a superoxo intermediate which is further reduced to the level of a peroxo species in[50] or before[38] the rate-determining step (see Introduction). The closeness of the observed [18]O KIEs for the enzyme reactions to the [18]O EIEs estimated for the end-on copper superoxo intermediates is consistent with a reversible O_2 binding step prior to substrate oxidation. As proposed in the present study, the [18]O EIE on the pre-equilibrium O_2 binding step may be the dominant contributor to the [18]O KIEs in the enzyme reactions. We hope to clarify this issue as well as the effects of subsequent redox chemistry on the [18]O KIEs using structurally defined CuO_2 complexes which react by ET or hydrogen atom transfer mechanisms.

This study has provided a method and series of benchmarks which can now be applied to studying how superoxide is processed by antioxidant enzymes such as Cu:Zn SOD (see above). A recent computational study of this enzyme[116] has predicted the formation of a formally $Cu^{II}-O_2^{-1}$ intermediate in the rate-limiting step for O_2 formation. This mechanism is fundamentally different than the one proposed here, where the rate-determining step is O_2 dissociation from a CuO_2 intermediate. We are currently examining the nature of the transition state in the Cu:Zn SOD reaction through measurements of [18]O KIEs on the oxidative and reductive processes.

Conclusions

A two-step, inner-sphere electron-transfer mechanism is proposed to describe the oxidation of $O_2^{\bullet-}$ to O_2 by coordinatively unsaturated copper(II) complexes. Kinetic measurements using stopped-flow UV−vis spectrophotometry indicate lower limits to the second-order rate constants of $\geq 1 \times 10^8$ M^{-1}s^{-1} at 20 °C which in some cases is up to 3 orders of magnitude faster than that expected from application of the Marcus Theory Cross Relation. On these grounds, an outer-sphere electron-transfer mechanism seems unlikely. In addition, low-temperature stopped-flow studies of the least oxidizing copper(II) complexes reacting with $O_2^{\bullet-}$ have provided evidence of a CuO_2 intermediate.

More compelling evidence for the formation of CuO_2 intermediates comes from studies of competitive oxygen kinetic isotope effects. These are, to our knowledge, the first measurements to be performed on reactions of $O_2^{\bullet-}$. The $^{16,16}k/^{18,16}k$ fall within a narrow range of 0.9836 to 0.9886 for reactions with copper(II) complexes. These complexes exhibit different

(110) Tian, G.; Klinman, J. P. *J. Am. Chem. Soc.* **1993**, *115*, 8891.
(111) Komiyama, K.; Furutachi, H.; Nagatomo, S.; Hashimoto, A.; Hayashi, H.; Fujinami, S.; Suzuki, M.; Kitagawa, T. *Bull. Chem. Soc. Jpn.* **2004**, *77*, 59.
(112) Chen, P.; Root, D. E.; Campochiaro, C.; Fujisawa, K.; Solomon, E. I. *J. Am. Chem. Soc.* **2003**, *125*, 466.
(113) Nakamura, A.; Tatsuno, Y.; Yamamoto, M.; Otsuka, S. *J. Am. Chem. Soc.* **1971**, *93*, 6052.
(114) Jazdzewski, B. A.; Reynolds, A. M.; Holland, P. L.; Young, V. G.; Kaderli, S.; Zuberbuehler, A. D.; Tolman, W. B. *J. Biol. Inorg. Chem.* **2003**, *8*, 381.
(115) Spencer, D. J. E.; Aboelella, N. W.; Reynolds, A. M.; Holland, P. L.; Tolman, W. B. *J. Am. Chem. Soc.* **2002**, *124*, 2108.
(116) Pelmenschikov, V.; Siegbahn, P. E. M. *Inorg. Chem.* **2005**, *44*, 3311.

coordination geometries and redox potentials which vary by 0.67 V. The observations of significantly inverse and driving-force independent kinetic isotope effects are inconsistent with simple $O_2^{\bullet-}$ binding as well as one-step electron-transfer mechanisms. Instead the results point toward a two-step mechanism where a CuO_2 intermediate is formed in a pre-equilibrium step prior to the rate-limiting loss of O_2. The small range of isotope effects implies that the CuO_2 intermediates formed from the different ligand complexes are structurally similar.

The resemblance of the CuO_2 intermediates formed from reactions of copper(II) complexes and $O_2^{\bullet-}$ to those generated from copper(I) and O_2 is supported by isotope effects calculated from stretching frequencies of structurally characterized CuO_2 adducts. These findings lay a foundation for using competitive oxygen isotope effects on reactions of biomimetic compounds to identify activated oxygen intermediates during catalysis by metalloenzymes.

Supporting Information Available: Experimental details and the description of equilibrium isotope effect calculations. This material is available free of charge via the Internet at http://pubs.acs.org.

JA056741N